Indonesian Journal of Electrical Engineering and Computer Science
Vol. 9, No. 2, February 2018, pp. 481~492
ISSN: 2502-4752, DOI: 10.11591/ijeecs.v9.i2.pp481-492

Improved Field-oriented Control for PWM Multi-level Inverter-fed Induction Motor Drives

D. L. Mon Nzongo[1], E. Leugoue[2], J. H. Zhang[3], G. Ekemb[4]
[1]SmartGrid and Sensor Technology, Institute of Fuzhou University, China
[2,3]Transmission & Distribution System Research institute, North China Electric Power University, China
[4]Department of Electrical Engineering, Quebec Chicoutimi University, Canada

Article Info

Article history:

Received 15 Nov, 2017
Revised Jan 10, 2018
Accepted Jan 29, 2018

Keywords:

Carrier based space vector pulse with modulation
Decoupling current control
D-q synchronous current
Field oriented control
Induction motor

ABSTRACT

This paper proposes a new approach to ensure the torque decoupled to the rotor flux of an induction machine based on the Field Oriented Control (FOC). The suggested method consists of inserting into the conventional d-q synchronous current controller, coupling terms of motor and multi-level inverter models. Making, the dynamic response of stator current components decoupled as well as the rotor flux and torque. In this paper, the mathematic model of an induction motor and multi-level inverter are first derived. Then, the synchronous current controller and modulation strategy for high power inverters are investigated. Finally, the validation through implementation and simulation of a 4.16 kV electric drive with MATLAB/Simulink and SimPowerSystems is performed. The model simulated in this paper includes an induction motor, nine-level cascaded H-bridge inverter and a carrier based space vector pulse-width-modulation. The results of the simulations of each method has been recorded and the comparison results reveal that the proposed method effectively maintains the rotor flux decoupled to the torque.

Corresponding Author:

D. L. Mon Nzongo,
SmartGrid and Sensor Technology Institute,
Fuzhou University, 2 Xueyuan Rd, 350108, Fuzhou, Fujian, China.
Email: monnzongodaniel@yahoo.fr

1. INTRODUCTION

During the last two decades, multi-level inverters have become very popular in high power motor drive applications such as fans, pumps, conveyors, traction and propulsion drives [1, 2]. They have these qualities since they are able to generate a stepped voltage waveform that better approximates a sinusoidal waveform. In high power drive applications, multi-level inverters provide to the induction motor a controlled voltage and frequency. Three traditional methods are available to manufacturers to control voltage and frequency of electric drives [1-6]. They are: (1) Scalar control, (2) Field-oriented Control (FOC) and (3) Direct Torque Control (DTC). Scalar control method consists to maintain the ratio voltage per frequency constant when controlling an induction machine. The FOC methods independently control the torque and flux component that includes coordinate transformation, Pulse Width Modulation (PWM) technique, and two synchronous controllers for the flux and torque components. The DTC methods are like FOC methods but require neither coordinate transformation nor PWM technique. They need a look-up table to select the suitable voltage vector of the inverter and a hysteresis control. [3-4] However, hysteresis controls are known to cause torque ripples in the motor and poor steady-state performance at low-speeds. This control mode has a fast response and a simple structure [7]. Moreover, they are vulnerable and can cause oscillation because of large values of stator/rotor resistance of the motor in high power drives.

In general, the main goal of FOC methods is to keep the oriented rotor flux decoupled to torque at any giving time by controlling the stator three-phase current [8-11]. This can be achieved by using speed

sensor measurement, coordinate transformation systems, estimation methods and synchronous regulators. But, the non-linear nature of the AC motors and three-phase inverters through their coupling terms, makes that goal difficult to achieve. Several improving methods of FOC were investigated in literature [12-15]. Among them, the stationary and synchronous frame PI regulators, additional PI type regulators are the most used [12, 13], this is because, they are based on a simple decoupling current control. Which is based on insertion into the synchronous current controller scheme coupling terms of the induction in the aim to suppress the nonlinear effects in the dynamic response of the stator current [14, 15]. However, these methods do not consider the coupling terms of the power inverter. It assumed as a gain during the design process and they compensate for its effects during the turning of the PI parameters. Hence the researched decoupling action between torque and flux is not accurately achieved practically [13].

In order to improve decoupling issues, this paper has proposed a new decoupling method that mainly consists of inserting into the synchronous current controller both effects of coupling terms due to the induction motor and multi-level inverter. Thus, the motor and the power inverter can be considered a first order system making the controller design easier.

This paper is organized into four sections. In the first section, the induction machine and inverter models are recalled. In the second section, the decoupling methods are presented. CB-SVPWM strategy for multi-level inverter is explained in the third section. Finally, simulation results through comparison are given.

2. MATHEMATICAL MODEL OF INDUCTION MOTOR FED BY PWM VSI INVERTER UNDER FOC CONTROL

2.1. Structure of the System Model

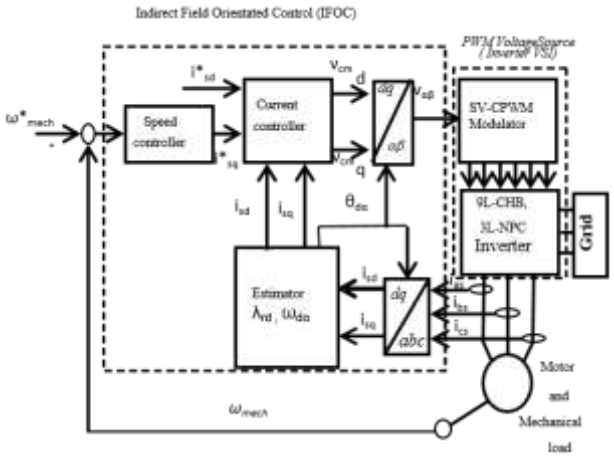

Figure 1. Basic Block Diagram of Field Oriented Control

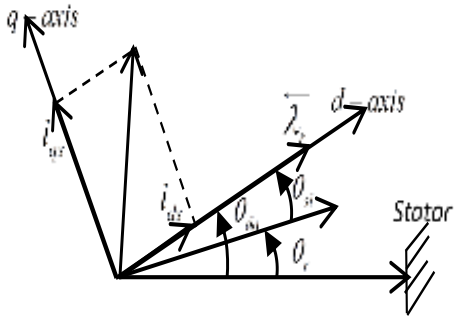

Figure 2. Principle of Field Oriented Control

2.2. Mathematical Models of Induction Motor and Inverter

The basic block diagram of FOC strategy for electric drive systems is shown in Figure 1. The basic principle of FOC is to control the speed or torque of an induction machine by only controlling the stator current of the induction machine [16,17]. In the case where only the speed is needed to be controlled (Figure1), the reference components of the current controller i_{sq}^{*} and i_{sq}^{*} are respectively obtained from the nominal flux and speed controller. The synchronous current controller compares these values to those measured from the three-phase current (i_a, i_b, i_c) and transformed to i_{sd} and i_{sq} . It generates the reference values of voltage components (v_{cm_d} and v_{cm_q}) that are transformed to the modulating signals (v_α and v_β) of the PWM modulator. The oriented rotor flux $\bar{\lambda}_r$ is localized from the stator by the angular θ_{da} (Figure 2). θ_{da} is estimated, and used with the coordinate transformation systems. The multi-level inverter is controlled by the PWM modulator and supply to induction machine a controlled voltage and frequency.

The dynamics of induction motor in the synchronously rotating d-q frame is given, such as in literature [1]:

$$\frac{dx}{dt} = Ax + Bu. \tag{1}$$

With A, B, x, u are described as it follows:

$$A = \begin{bmatrix} a_{11} & a_{12} & a_{13} & a_{14} \\ -a_{12} & a_{11} & -a_{14} & a_{13} \\ a_{31} & 0 & a_{33} & a_{34} \\ 0 & a_{31} & -a_{34} & a_{33} \end{bmatrix} B = \begin{bmatrix} b_1 & 0 \\ 0 & b_1 \\ 0 & 0 \\ 0 & 0 \end{bmatrix} x = \begin{bmatrix} i_{sd}^e \\ i_{sq}^e \\ \lambda_{rd}^e \\ \lambda_{rq}^e \end{bmatrix}$$

$$a_{11} = -\frac{R_s}{s L_s} - \frac{L_m^2}{s L_s L_r t_r}, \quad a_{12} = w_{da}, \quad a_{31} = \frac{L_m}{t_r}, \quad a_{33} = -\frac{1}{t_r}, a_{34} = w_{sl},$$

$$a_{13} = -\frac{L_m}{s L_s L_r t_r}, \quad a_{14} = -w_r \frac{L_m}{s L_s L_r}, \quad b_1 = \frac{1}{s L_s}, \quad b_2 = 1 - \frac{L_m^2}{s L_s}.$$

Under FOC, λ_{rq} is zero at the steady state, and the rotor field oriented control is achieved when $l_{rd} = \left| \overset{\mathrm{r}}{l}_{rd} \right|$ is constant [9]. So, from equation (1) the stator voltage components in synchronous frame are derived as:

$$v_{sd} = R_s i_{sd} + s L_s \frac{di_{sd}}{dt} + \frac{L_m}{L_r} \frac{dl_{rd}}{dt} - w_{da} s L_s i_{sq} \tag{2}$$

$$v_{sq} = R_s i_{sq} + s L_s \frac{di_{sq}}{dt} + w_{da} \frac{L_m}{L_r} l_{rd} + w_{da} s L_s i_{sd} \tag{3}$$

$$\lambda_{rd} = L_m i_{sd} \tag{4}$$

$$T_{em} = \frac{p}{2} \frac{L_m}{L_r} i_{sdref} i_{sq} \tag{5}$$

Equations (2) to (5) represent the mathematical model of the induction machine in synchronous frame under FOC. Concerning the power inverter, which is the multi-level inverter, its model is obtained in this paper by taking into account all the time delay existing to manage the power flow between the supply and the induction motor. These time delays are due to the digital processing board, measuring and filtering devices T_{mes} $\mathrm{T_{meas}}$ gate drivers and death time units T_{driver}. The total delay time due to multi-level inverter is:

$$T_{VSI} = T_r + T_E / 2 + T_{driver} + T_{meas} \tag{6}$$

Thus, dynamical model of multi-level inverter is:

$$v_{sd} = \left(v_{sd_{cm}} - v_{sd} + w_{da} T_{VSI} v_{sq} \right) \frac{K_{VSI}}{s T_{VSI}} \tag{7}$$

$$v_{sq} = \left(v_{sq_{cm}} - v_{sq} - w_{da} T_{VSI} v_{sd} \right) \frac{K_{VSI}}{s T_{VSI}}. \tag{8}$$

Where $v_{sd_{cm}}, v_{sq_{cm}}$ are synchronous d-q voltages delivered by the FOC. K_{VSI} represents the gain of inverter. According to (2), (3), (7), (8) the model of an induction motor fed by the multi-level inverter is represented in Figure 3.

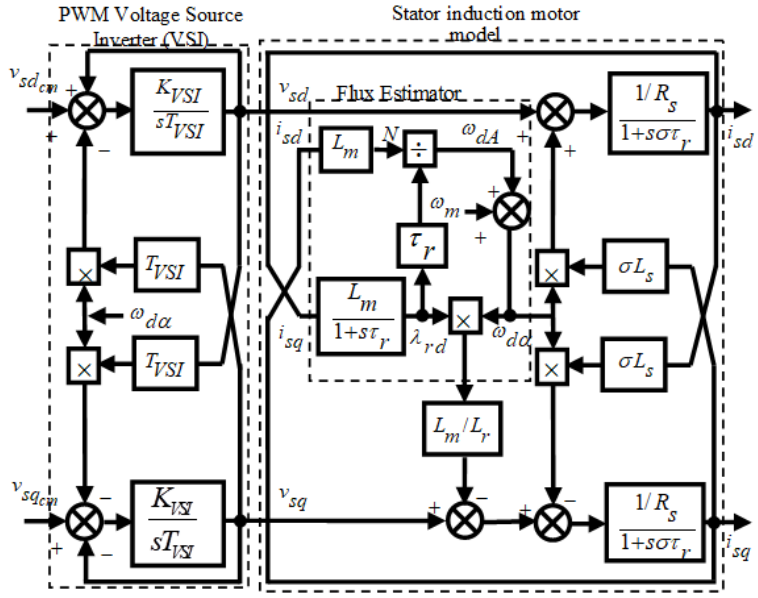

Figure 3. Block Diagram of an Induction Motor Fed by A PWM Inverter

From Figure 3, the controlled voltage is applied to the induction motor through the power inverter. Observing this Figure 3, the voltage in d and q axis contents nonlinearities which are coupling terms through the model of the power inverter and induction machine. Therefore, d and q-axis current components are strongly dependent each other [10, 12, 13]. Thus, independently controlling the current in d and q axis can be achieved by either using fed-forward methods or decoupling approaches.

3. SYNCHRONOUS DECOUPLING CURRENT CONTROLLER

The plant model of an IM motor and power inverter under FOC has been represented in Figure 3. It shows the nonlinearity of the induction motor that introduce coupling between the synchronous current components. Thus, any change of one of these components may affect the dynamic of the entire system [17-20].

3.1. Conventional decoupling controller

The current components of dynamic equations through the induction motor are simplified as:

$$s L_s \frac{di_{sd}}{dt} = - R_s i_{sd} + w_{da} s L_s i_{sq} + v_{sd} \quad (9)$$

$$s L_s \frac{di_{sq}}{dt} = - R_s i_{sq} - w_{da} L_s i_{sd} + v_{sq} \quad (10)$$

In the d and q axis, the coupling terms between the two axes are respectively defined by $w_{da} s L_s i_{sq}$ and $w_{da} L_s i_{sd}$; when the inverter model is not considered.

The diagram block of the conventional decoupling current controller with the synchronous voltages to be applied to the induction motor is represented in Figure 4. The power inverter is assumed to be ideal so its model does not appear. This current controller is easier to be implemented using analogical or digital circuits but as it has been mentioned above, the expected decoupling feature is not achieved.

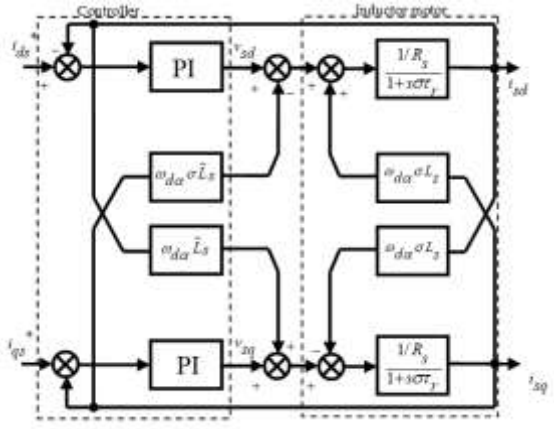

Figure 4. The Block Diagram of Conventional Decoupling PI Controller.

From Figure 4, the decoupling is accomplished by choosing voltage commands such as :

$$v_{sd}^{*}=\left(K_p+\frac{K_i}{s}\right)\left(i_{sd}^{*}-i_{sd}\right)-\omega_{da}\overline{\sigma}\overline{L}_s i_{sq} \tag{11}$$

$$v_{sq}^{*}=\left(K_p+\frac{K_i}{s}\right)\left(i_{sq}^{*}-i_{sq}\right)-\omega_{da}\overline{L}_s i_{sd} \tag{12}$$

where, $K_p, K_i>0$ is the proportional and integral gain and $\overline{\sigma},\overline{L}_s$ are respectively the estimated values of σ, L_s .

3.2. Proposed synchronous decoupling current controller

Previously the decoupling was achieved by adding to the PI controller just the coupling terms due to induction motor. However, it has been demonstrated through the modeling of motor and inverter that, coupling terms exist due to the induction motor and power inverter (Figure 3). Figure 5 shows the proposed decoupling current controller. The basic idea of the proposed decoupling network (DN) is to also consider the presence of the nonlinearity of the power inverter into the current controller. Therefore, the decoupling current is then accomplished by choosing voltage commands such as:

$$v_{sd_{cm}}=\left(K_p+\frac{K_i}{s}\right)\left(i_{sd}^{*}-i_{sd}\right)-\overline{\sigma}\overline{L}_s\omega_{da}i_{sq}-\omega_{da}T_{VSI}v_{sq} \tag{13}$$

$$v_{sq_{cm}}=\left(K_p+\frac{K_i}{s}\right)\left(i_{sq}^{*}-i_{sq}\right)+\omega_{da}\frac{\overline{L}_m}{\overline{L}_r}\overline{\lambda}_{rd}+\overline{L}_s\omega_{da}i_{sd}+\omega_{da}T_{VSI}v_{sd} \tag{14}$$

Where the decoupling terms are equal to

$$v_{sd,comp}=-\overline{\sigma}\overline{L}_s\omega_{da}i_{sq}+\frac{\overline{L}_m}{\overline{L}_r}\frac{d\overline{\lambda}_{rd}}{dt}-\omega_{da}T_{VSI}v_{sq} \tag{15}$$

$$v_{sd,comp}=\omega_{da}\frac{\overline{L}_m}{\overline{L}_r}\overline{\lambda}_{rd}+\overline{\sigma}\overline{L}_s\omega_{da}i_{sd}+\omega_{da}T_{VSI}v_{sd} \tag{16}$$

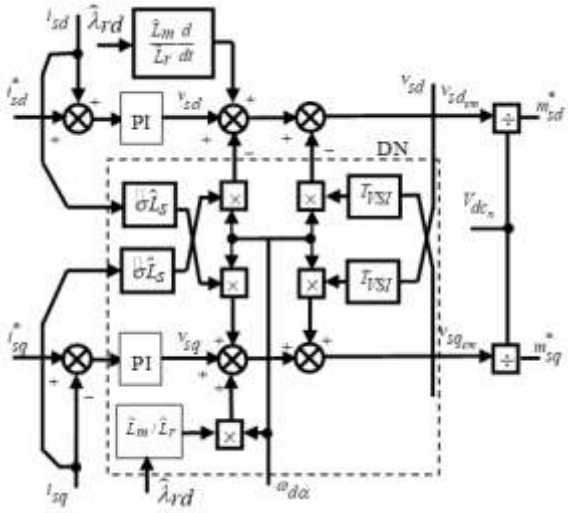

Figure 5. The Block Diagram of Proposed Decoupling PI Controller.

From the above analysis, the model of the induction motor and power inverter are not represented in Figure 5 for the reasons of clarity. The new decoupling network (DN) is highlighted by the dashed square in Figure 5. The Figure 6 and Figure 7 are simulation results of FOC using the d-q representation of the inverter and induction motor. The inverter total delay time is $T_{VSI} = 1ms$ and the gain is $K_{VSI} = 1$. $k_{pi} = 8.6$ and $k_{ii} = 530$ are respectively the proportional and integral gain of synchronous current controller. The motor parameters are shown Table I. Also, it has been initialized as follows: $I_{sd0} = 17.4A$, $I_{sq0} = 1.245kA$, $\omega_{mech0} = 124.5rad/s$.

Table 1. Motor Specifications and Parameters

Squirrel Cage Induction motor (50Hz)	
Rated Power	1250 *hp*
Rated voltage	4160 V
Pair of poles	2
Stator resistance	0.21 Ω
Rotor resistance	0.146 Ω
Stator leakage inductance	5.2
Rotor Leakage inductance	5.2 *mH*
Magnetizing inductance	155 *mH*

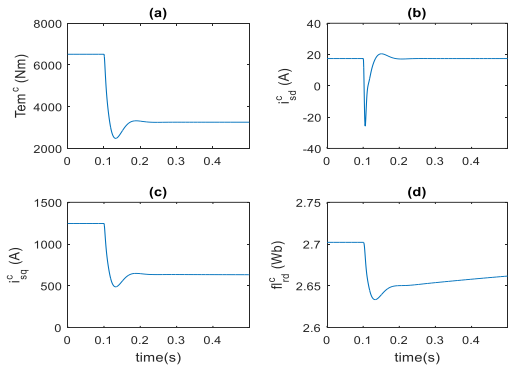

Figure 6. Numerical Simulation of D-Q Model of FOC based Conventional Decoupling PI Controller. (a) Electromagnetic Torque. (b) D-Axis Current. (c) Q-Axis Current. (d) Rotor Flux

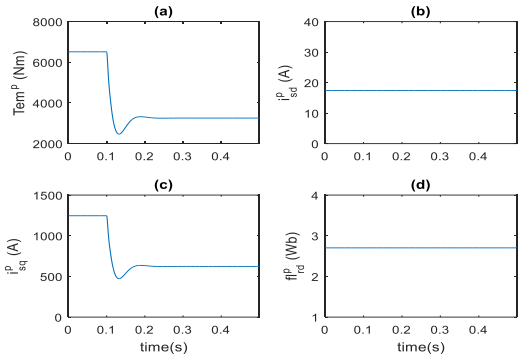

Figure 7. Numerical Simulation of FOC based Proposed Decoupling PI Controller.(a) Electromagnetic Torque. (b) D-Axis Current. (c) Q-Axis Current. (d) Rotor Flux. Space Vector Carrier based Modulation for Multilevel Voltage Source Inverter

The results shown in Figure 6 and Figure 7 are the dynamic responses of flux, synchronous current components and torque obtained during a step change in the load torque at 0.1s from T_{em0} to $T_{em0}/2$. In Figure 6, the results were obtained when considering the conventional approach represented in Figure 4. The torque disturbance appeared at 0.1s has directly influenced the transient states of rotor flux ($\lambda_{rd} = fl^{c}_{rd}$) and the two synchronous current components (i^{c}_{sd}, i^{c}_{sq}) and also the emitted torque T^{c}_{em}. This behavior shows how all the parameters are influenced by the disturbance of load torque appeared in q-axis. As concluded, the axes are still coupled.

In Figure 7, the suggested approach was considered. The same disturbance occurred at 0.1s does not change the behavior of the rotor flux ($\lambda_{rd} = fl^{p}_{rd}$) and the current located in d-axis (i^{c}_{sd}) as previously. But in the same time, the dynamic behavior of the current in the q-axis (i^{p}_{sq}) and the emitted (T^{p}_{em}) torque are obviously affected and have kept the same behavior as in Figure 6. Thus, the decoupling is achieved. The torque is then controlled while the flux is kept at the initial value.

4. MULTI-LEVEL INVERTERS FOR HIGH POWER ELECTRIC DRIVE SYSTEMS

Figure 8 represents systematic topologies of multi-level inverter available in industry. Figure 8a is a diagram of three-level neutral point clamped (NPC) supplying a high-power induction motor. The NPC inverter is itself supplied through a twelve-pulse uncontrolled rectifier associated to a shifted three-phase transformer. Each leg of NPC inverter is constituted of four isolated gate base transistors (IGBTs) and two clamping diodes [21-23].

Figure 8.b is a nine-level cascaded H-bridge. It is constituted of four modules of H-bridge inverter connected in series. Each module is supplied by a three-phase rectifier. The rectifiers of each H-bridge are separately supplied to the electric grid through a shifted multi-winding transformer. The switching states of the H-bridge cell can be found in [1], [21-23]. A full H-bridge cell of each leg provides three levels of voltage (e.g. -1, 0, 1) as three three-level NPC. Nine-level voltage is obtained by consecutively connecting in serial the partial H-bridge cells of each leg.

The voltage position is obtained from the voltages V_{α} and V_{β} (see Figure 1). In general, the total output voltage position that can be generated by a multi-level inverter is obtained by $V_{sp} = (n_{level})^3$. Where n_{level} is the inverter number of the level. If n_{level} is respectively three-level and nine-level, the possible output voltage positions are respectively 27 and 729. The voltage position can be represented in $\alpha - \beta$ frame. It is used to determine the switching instance of multi-level inverter, as well as the corresponding switching devices to turn 'on' or 'off'. The spatial vector of three and nine-level inverters are shown in Figure 9a and Figure 9b. From these figures, it can be concluded that the nine-level inverter is more complex to control than the three-level.

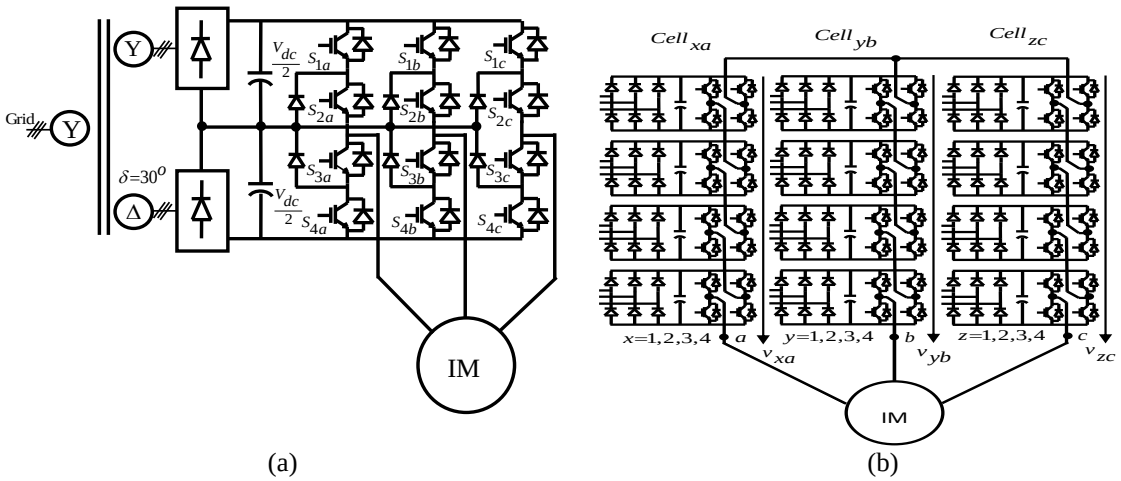

(a) (b)

Figure 8. Multi-level Inverter Topologies: (a) Neutral Point Clamped (NPC), (b) Series-connected H-bridge (CHB)

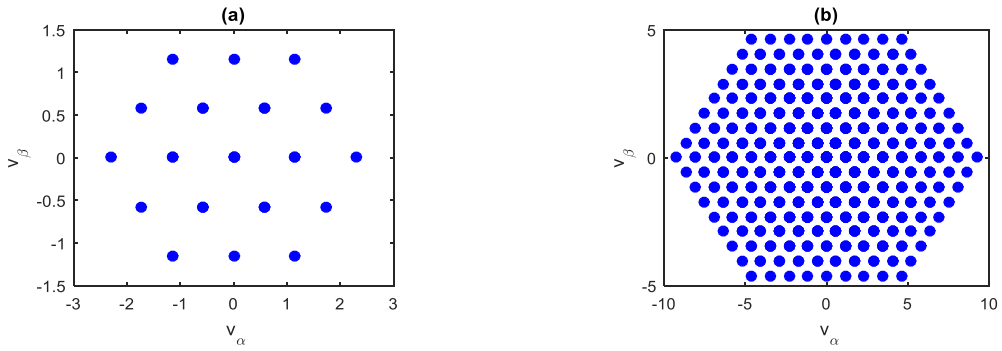

Figure 9. Space Vector Representation of Output Voltage of Multi-level Inverter.
(a)Three-level, (b) Nine-level.

The minimum DC-link voltage requiring by multi-level inverter is obtained from the desired output line to line voltage (V_{llrms}). It can be calculated as:

$$V_{dc_n} = \frac{1}{n_{level} - 1}\sqrt{2}V_{llrms} \tag{17}$$

where V_{dc_n} is DC-link voltage, V_{llrms} is line to line voltage of induction motor which represents the maximal voltage that can be generated by the multi-level inverter. In the case of three and nine-level inverters shown in Figure 6 and Figure 7 and considering the induction motor line to line voltage equal to $V_{llrms} = 4.16kV$ the minimum dc-link voltage is respectively $V_{dc_{3L-NPC}} = 5883V$ and $V_{dc_{3L-NPC}} = 1470V$. Thus, the DC-link voltage of the multi-level inverter decreases when the number of level increases.

4.1. Principle of carrier based space vector pulse wide modulation for multi-level inverter

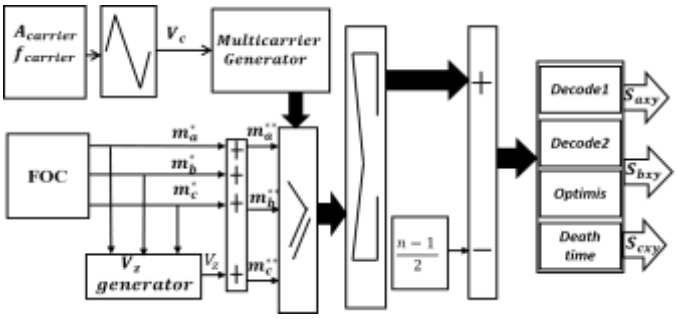

Figure 10. Basic Block Diagram of CB-SVPWM Modulation Strategy

A carrier based space vector pulse-width-modulation (CB-SVPWM) represented in Figure 10 is an equivalency of space vector pulse-width modulation (SVPWM) [1,23]. The principle of CB-SVPWM consists to generate $N_{level} - 1$ carrier waves and to compare them at each time to a set of three-phase modulating voltage m_a^*, m_b^*, m_c^*. These carriers are vertically phase shifted, and are disposed in continues bands around the reference zero. The results of the comparison are then decoded and optimized in order to generate the correct gate signals (CBPWM principle). With the induction motor, where the neutral point is floating, a zero-sequence component V_z can be calculated from the modulating three-phase signals and added to the same signal to define the modified reference $m_a^{**}, m_b^{**}, m_c^{**}$.Therefore the new comparison result generates the correct gate signals conform to CB-SVPWM modulation. The modulation index M and the frequency index M_f are defined by equations (18) and(19). The zero-sequence component is defined by the

equation (20). A_c , f_c are respectively the amplitude and frequency of the carrier voltage of the reference voltage coming from the FOC side (Figure 1).

The waveforms of CB-SVPWM generated using Simulink common blocks and Matlab embedded function blocks are shown in Figure 11.

$$M = \frac{A_m^*}{A_c} \tag{18}$$

$$M_f = \frac{f_c}{f_{cm}} \tag{19}$$

$$V_z = \frac{\left[\max(m_a^* + m_b^* + m_c^*) + \min(m_a^* + m_b^* + m_c^*)\right]}{2} \tag{20}$$

$$m_a^{**} = m_a^* - v_z, m_b^{**} = m_b^* - v_z, m_c^{**} = m_c^* - v_z \tag{21}$$

The waveforms of CB-SVPWM generated using Simulink common blocks and Matlab embedded function blocks are shown in Figure11. Figure11a and Figure11b are multi-carrier and references waveforms generated for three and nine-level inverter. They are output voltage of three and nine-level inverter topologies configured as in Figure8. The results obtained in Figure11a and Fig11c are equivalent to those obtained with SVPWM in the literature. While those obtained in Figure11b and Figure11d are known as CBPWM. The inverter with nine-level generates output voltage waveforms close to the sine reference. So, less harmonics are propagated in the windings of the induction motor. It considerably reduces power losses inside the induction motor and cables as well as the torque ripples.

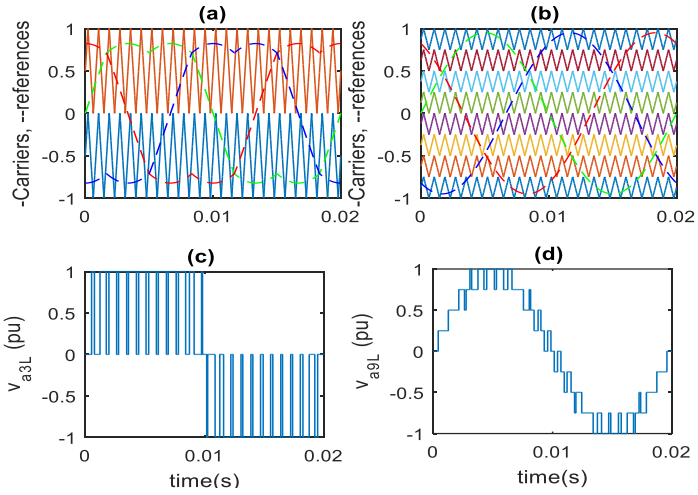

Figure 11. Generation of Waveforms of CB-SVPWM. (a)-(b): carrier and reference signal of three and nine-level inverter. (c)- (d): phase a voltage of three and nine-level inverter

5. SIMULATION RESULTS

To verify the proposed decoupling current control scheme, SimPowerSystems toolbox has been used to implement a 4.16 kV induction motor supplied by a nine-level CHB inverter. The decoupled current controllers previously designed and simulated have been used to this simulation. The CB-SVPWM has been implemented as presented above. The whole drive has been configured as shown in Figure 1. The parameters of the motor are kept as shown in Table I.

As it has been mentioned, the main objective of this simulation is to compare the two decoupling current control approaches during a step change in the load torque at 0.1s from T_{em0} to $T_{em0}/2$. And the comparison is then achieved by observing the transient of the rotor flux component (λ_{rd}^c , λ_{rd}^p) and electromagnetic torque (T_{em}^c , T_{em}^p) as shown in Figure 12.

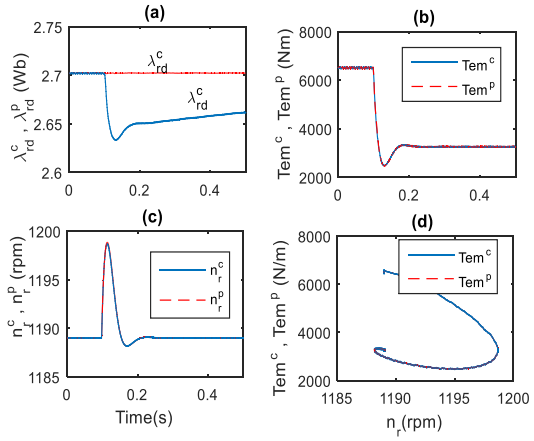

Figure 12. Simulation comparison of conventional ($.^{c}$) and proposed ($.^{p}$) decoupled current controller for FOC of induction motor supplied by multi-level inverter. (a) Rotor flux (λ_{rd}^{c}, λ_{rd}^{p}), (b) electromagnetic torque (Tem^{c}, Tem^{p}), (c) rotating speed (n_r^{c}, n_r^{p}), (d) $Tem = f(n_r)$.

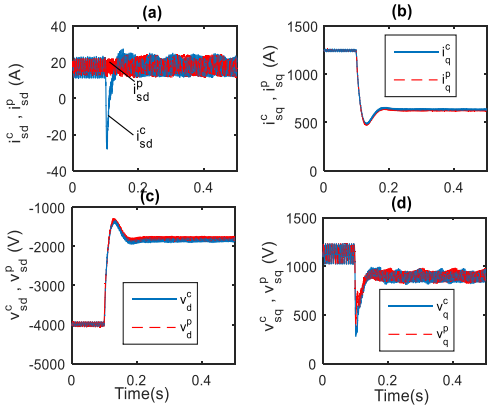

Figure13. Simulation comparison of conventional ($.^{c}$) and proposed ($.^{p}$) decoupled current controller for FOC. (a) d-axis stator current (i_{sd}^{c}, i_{sd}^{p}), (b) q-axis stator current (i_{sq}^{c}, i_{qd}^{p}), (a) d-axis stator voltage (V_{sd}^{c}, V_{sd}^{p}), (b) q-axis stator current (i_{sq}^{c}, i_{qd}^{p})

Because of the control principle, stator current components in synchronous frame (Figure 13a and Figure 13b) has been measured for each case, and are noted (i_{sd}^{c}, i_{sq}^{c}) for the conventional approach and (i_{sd}^{p}, i_{sq}^{p}) for the proposed approach. In the same manner the voltage components in synchronous frame (v_{sd}^{c}, v_{sq}^{c}) and (v_{sd}^{p}, v_{sq}^{p}) have been also measured and are represented in Figure 13c and Figure 13d.

The corresponding three-phase and current of synchronous current and voltage are measured through the windings of a 4.16kV induction motor and are represented respectively in Figure 14a-b and Figure 15a-b. Finally, dynamic value of current $\delta_{ia} = i_{sa}^{p} - i_{sa}^{c}$ and voltage $\delta_{vas} = v_{sa}^{p} - v_{sa}^{c}$ compensation has respectively been recorded as shown in Figure 14c and Figure 15c. Observing these figures, following conclusions can be made: (1) the proposed approach effectively decouples the flux to the torque by maintaining the current i_{sd}^{p} invariant during the variation of the load torque.

This can be seen through Figure 12a and Figure 13b; (2) when the decoupling is achieved, only the d-axis current and flux are different to the value obtained using the conventional approach. This means the torque emitted, rotating speed are the same for both method (Figure 12 and Figure 13); (3) in a-b-c $\delta_{ia} = i_{sa}^{p} - i_{sa}^{c}$ in Figure 14c and $\delta_{vas} = v_{sa}^{p} - v_{sa}^{c}$ prove the contribution in term of current and voltage of the suggested approach.

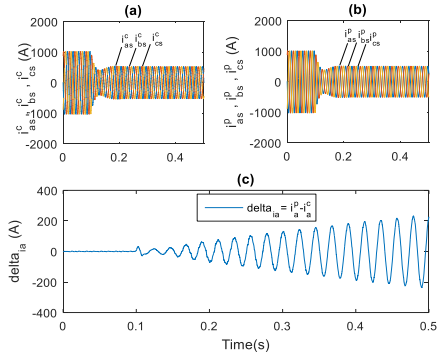

Figure 14. Simulation comparison of conventional ($.^{c}$) and proposed ($.^{p}$) decoupled current controller for FOC. (a)-(b) three-phase stator current (i_{as}^{c}, i_{bs}^{c}, i_{cs}^{c}) and (i_{as}^{p}, i_{bs}^{p}, i_{cs}^{p}), (c) current of compensation $\delta_{ia} = i_{as}^{p} - i_{as}^{c}$.

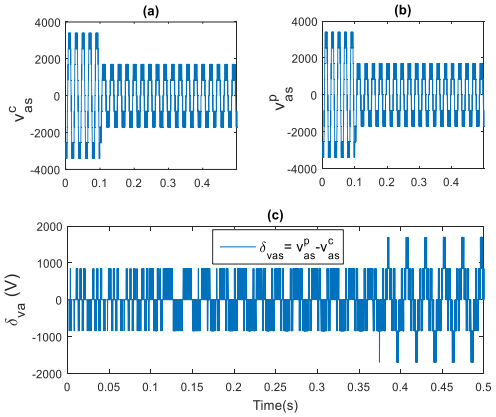

Figure 15. Simulation comparison of conventional ($.^{c}$) and proposed ($.^{p}$) decoupled current controller for FOC. (a)-(b) three-phase stator voltage (v_{as}^{c}, v_{bs}^{c}, v_{cs}^{c}) and (v_{as}^{p}, v_{bs}^{p}, v_{cs}^{p}), (c) voltage of compensation $\delta_{vas} = v_{as}^{p} - v_{as}^{c}$.

6. CONCLUSION

This paper has presented an approach to improve FOC of an induction machine supplied by multi-level inverter. The main contribution of this paper is the suggestion to insert coupling terms of power electronic inverter into the decoupling synchronous current controller in order to ensure decoupling between the components located in d and q axis. This can gain advantages since all the drives became equivalent to a first order system and the control parameter are easier to design. In the first section of this paper, the model of an induction motor and multi-level inverter are recalled. In the second section, the conventional decoupling current control strategy applied to reduce the coupling between the rotor torque and flux is explained. Then the limit of this approach is presented and improved by adding coupling terms of motor and multi-level inverter. In the third section, multi-level inverter topologies and CB-SVPWM are presented. Finally, to verify the method proposed, two simulation models were implemented using MATLAB/Simulink. The first model is a d-q representation of induction motor and inverter fed by decoupling current controllers. The second model is based on physical models of 4.16kV induction motor and nine-level CB-SVPWM inverter implemented using SimPowerSystems. In the last section, the results of simulation by comparing the two approaches were presented and have proved the necessity to insert coupling terms of the motor and power inverter into the synchronous current controller.

REFERENCES

[1] Bin Wu, "High Power Converters and AC Drives". Hoboken, NJ, USA: John Wiley & Sons, 2006, pp. 253-266.
[2] S. H. Asgari, M. Jannati, T. Sutikno, N. Rumzi, and N. Idris, "Vector Control of Three-Phase Induction Motor with Two Stator Phases Open-Circuit, " vol. 6, no. 2, 2015.
[3] G. Garcia, R. Stephan, and E. Watanabe, "Comparing the indirect field oriented control with a scalar method," *IEEE Trans. Ind. Electron.*, vol.41, pp. 201–207, 1994.
[4] R. Rajendran, "A Comparative Performance Analysis of Torque Control Schemes for Induction Motor Drives," vol. 2, no. 2, pp. 177–191, 2012.
[5] T.A. Wolbank, A. Moucka, J.L. Machl, "A Comparative Study of Field-Oriented Control and Direct-torque Control of induction Motors reference to shaft-sensorless Control at Low and Zero-Speed,", *IEEE International Symposium on Intelligent Control*, Oct. 2002, pp. 391-396.
[6] J. A. Santisteban and R.M. Stephan, "Vector Control Method for induction Machines: an overview," *IEEE Trans. On Educ.*, vol. 44, no. 2, pp. 170-174, 2001.
[7] D. Ming, T. T. Yong-qi, S. Hai-liang, and W. Bing-jie, "Study of an Improved Fuzzy Direct Torque Control of Induction Motor," vol. 11, no. 4, pp. 691–698, 2013.
[8] Z. Daboussi, N. Mohan, "Digital Simulation of Field-Oriented Control of induction motor drives using EMTP," *IEEE Trans. Energy, Convers.*, vol.3, no. 3 Sept. 1988, pp. 667–673, 1988.
[9] M. Comanescu, Longa Xu, Todd D. Batzel, "Decoupled Current Control of Sensorless Induction-Motor Drives by Integral slidding Mode," *IEEE Trans. Ind.Appl.*, vol. 55, no. 11, pp. 3836-3845, Aug./Oct. 2008.
[10] G. Wang, Yong Yu, R. Yang, Wei Cheng, and D. Xu, "A Robust Speed Controller for Speed Sensorless Field-Oriented Controller Induction Motor Drives," *in Proc. IEEE VPPC*, Harbin, China. Sept. 3-5, 2008, pp. 978-981.

[11] M.S. Naft Sard, M.E.H. Benbouzid, "Induction Motors Direct Field Oriented Control with Robust On-Line Tuning of Rotor Resistance," *IEEE Trans. Energy, Convers*., vol.14, no. 4 Dec. 1999, pp. 1038–1042, 1999.
[12] J. Jung, S. Lim, and K. Nam, "PI Type decoupling control scheme for high speed operation of induction motors," *in Proc. IEEE PESC*, Jun. 22-27,1997, vol. 2, pp. 1082-1085.
[13] R. J. Wai and Kuo-Min Lin, "Robust Decoupled Control of Direct Field-Oriented Induction Motor Drive", *IEEE Trans. Ind. Electron*., vol. 52, no. 3, pp. 837-852, Jun. 2005.
[14] C. E. Maucary, E. Mendes, "Decoupled Direct Control for PWM Inverter-Fed Induction Motor Drives", *IEEE Trans. Ind.Appl*., vol. 38, no. 5, pp. 3836-3845, Jan./Feb. 1998.
[15] T. M. Roman and R. J. Kerkman, "A New Synchronous Current Regulator and Analysis of Current-Regulated PWM Inverters", *IEEE Trans. Ind.Appl*., vol. IA-22, no. 4, pp. 678-690, 1986.
[16] D. M. Bord and D. W. Novotny, "New Control of VSI-PWM Inverters", *IEEE Trans. Ind.Appl*., vol. IA-21, no. 4, pp. 562-570, 1985.
[17] F. Briz, M. W. Degner, and R. D. Lorenz, "Analysis and design of current regulators using complex vectors," *IEEE Trans. Ind.Appl*., vol. 36, no. 3, pp. 817-825, May/Jun. 2000.
[18] R.D. Lorenz and D.B. Lawson, "A simplified Approach to continuous On-Line Tuning of Field-Oriented Induction Machine Drives," *IEEE Trans. Ind.Appl*., vol. 26, no. 3, pp. 420-424, 1999.
[19] Dong-Choon Lee, Seung-Ki Sul and Min-Ho Park, "High Performance Current Regulator for a Field-Oriented Controlled Induction Motor Driver", *IAS Trans. conf.Rec*., pp. 538-544, 1992.
[20] H.W. Van Der Brock, H.C. Skudelny and G.V. Stanke, "Analysis and Realization of a Pulse Width Modulation Based on Voltage Space Vector," *IEEE, Trans., Ind. Appl*., vol. 24, no. 1, pp. 142-150, 1988.
[21] A. Nabae, I. Takahashi, H. Akagi, "A New Neutral Point Clamped PWM Inverter", *IEEE Trans. Ind. Appl*. vol. 1A-17, pp. 518-522, 1981.
[22] Schibli, N., Nguyen, T., Rufer, A "Three phase multilevel converter for high-power induction motors," *IEEE, Trans., Power Elect*., vol. 13, no. 5, pp. 978-986, 1998.
[23] Carrara, G., Gardella, S., Marchesoni, M., Salutari, R., "Sciutto, G, A new multilevel PWM method: a theoretical analysis". *IEEE, Trans., Power Elect*., vol. 7, no. 3, pp. 497-505, 1992.